

Quantitative Determination of the Mechanical Properties of Nanomembrane Resonators by Vibrometry In Continuous Light

Fan Yang,^{*} Reimar Waitz,[†] and Elke Scheer

Department of Physics, Universität Konstanz, 78464 Konstanz, Germany

We present an experimental study of the bending waves of freestanding Si_3N_4 nanomembranes using optical profilometry in varying environments such as pressure and temperature. We introduce a method, named Vibrometry in Continuous Light (VICL) that enables us to disentangle the response of the membrane from the one of the excitation system, thereby giving access to the eigenfrequency and the quality (Q) factor of the membrane by fitting a model of a damped driven harmonic oscillator to the experimental data. The validity of particular assumptions or aspects of the model such as damping mechanisms, can be tested by imposing additional constraints on the fitting procedure. We verify the performance of the method by studying two modes of a 478 nm thick Si_3N_4 freestanding membrane and find Q factors of 2×10^4 for both modes at room temperature. Finally, we observe a linear increase of the resonance frequency of the ground mode with temperature which amounts to 550 Hz/°C for a ground mode frequency of 0.447 MHz. This makes the nanomembrane resonators suitable as high-sensitive temperature sensors.

I. INTRODUCTION

Nanomechanical membranes are extensively used in a variety of applications including among others high frequency microwave devices [1], human motion detectors [2], and gas sensors [3]. Membranes of manifold materials such as silicon, siliconnitride, siliconcarbide, mono-/multi-layers of graphene, and transition metal dichalcogenides (e.g., molybdenumdisulfide) have been recently studied regarding their nanomechanical properties [4–11]. Membranes inside an optical cavity allow a coherent coupling of optical and mechanical degrees of freedom. This opens up fascinating possibilities for studying the boundary between classical and quantum physics [12, 13], such as optical cavity cooling [14], ultra precise mass spectrometry [15, 16] and many more. Different nanostructures can be processed on membranes which can be patterned laterally by using dry etching or focused ion beam techniques (e.g., for realizing phonon wave guides [17]).

The Q factors of different vibration modes of commercial high- Q siliconnitride membranes ranging from 10^6 to 10^7 at low temperatures have been reported [18–20]. The resonance frequency is sensitive to the environment temperature [9]. The exploration of the temperature dependent mechanical properties of membranes is particularly important because it provides the possibility to control the mechanical properties of nanomembrane devices. Liu et al. [9] found that time-dependent modulation of the heating provided by laser irradiation, promotes rapid energy exchange between coupled vibration modes, thereby tuning the mechanical mode frequencies by more than 12% by optical heating.

Depending on the material, the thickness, the lateral size of the membrane, and the excitation state, the eigen-

frequencies of bending waves of nanomembranes may range from a few kHz to several 100 MHz [6], those of thickness oscillation may even exceed 100 GHz [21], requiring a versatile excitation and detection method able to operate in this wide frequency range and to resolve small vibration amplitudes in the nanometer range. Optical interferometry in combination with piezoelectric excitation is such a method [6]. With this method we also achieved the spatially resolved measurement of the stress tensor in thin membranes using bending waves [22]. However, the interferometer detects the response of the complete system consisting of the excitation system and the membrane under study. In general, the excitation system may also show resonances in a wide frequency range of the membrane vibrations. Therefore we developed a method called Vibrometry In Continuous Light (VICL) with customized scripts to decompose the total response into the contributions of the membrane and of the excitation system. Through this method the eigenfrequencies and Q factors of the membrane can be characterized.

II. EXPERIMENT

The membranes are fabricated using wet etching in aqueous potassium hydroxide (KOH). A 0.5 mm thick commercial (100) silicon wafer which both sides are coated with a layer of silicon nitride is applied. Silicon nitride layers with different thickness can be applied on silicon wafers. The membrane is fabricated on the front layer, and the backside layer serves as an etching mask. Laser ablation is used to open the etching mask with a typical size of $1 \times 1 \text{ mm}^2$. Membranes with different sizes can be obtained by controlling the size of opened etching masks. Using anisotropic etching in KOH, a hole is etched through the openings of the mask. After about twenty hours the KOH solution reaches the topside layer and a membrane is formed, supported by a massive silicon frame. The cross section of a free-standing silicon

^{*}Electronic address: fan.yang@uni-konstanz.de

[†]Now at: RATIONAL AG, Iglinger Str. 62, 86899 Landsberg am Lech, Germany

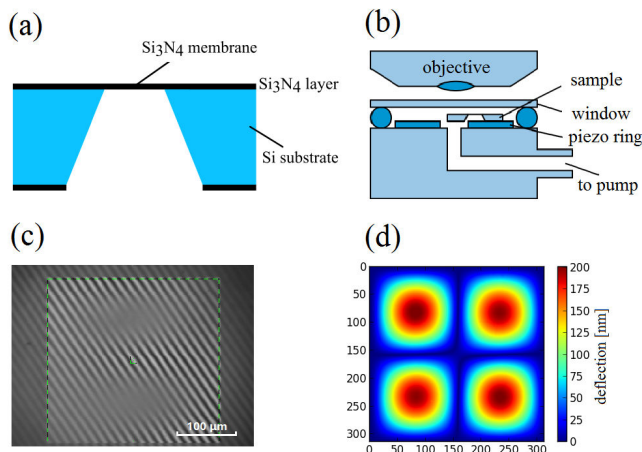


FIG. 1: (a) Cross section of a free-standing silicon nitride membrane supported by a 0.5 mm thick silicon substrate. (b) Sketch of the measurement setup showing the membrane chip, the piezo ring, the vacuum chamber and the objective is shown above. Pressures from 10^{-2} mbar to 10^2 mbar can be applied. (c) Camera view of a $298 \times 296 \mu\text{m}^2$ membrane under the imaging interferometer objective using continuous light. Resonance vibration measurement area is indicated by the green frame. Here the membrane is in the (1,2) mode, as indicated by the blurring of the almost diagonal interference lines. (d) False color image of an amplitude profile of the membrane recorded at an excitation frequency of 909 kHz by the interferometer, corresponding to the (2,2) mode. For this picture the membrane oscillation is driven in the nonlinear regime. The height of the area at the boundary of the membrane and along the nodes (dark blue) is close to 0 nm, the maximum amplitude of the centers of the excited mode (dark red) is nearly 200 nm.

nitride membrane supported by a silicon substrate is presented in Fig. 1(a).

The chip carrying the membrane is glued to a piezo ring, and the piezo is then glued to a massive brass block. Bending waves of the membranes are excited by applying an AC voltage V_{AC} to the piezo. The sample is placed in a vacuum chamber connected to a pressure controller (see Fig. 1(b)), so we have full control over the pressure of the surrounding atmosphere in a pressure range from $p = 0.001$ mbar to atmospheric pressure. Analysis in the below we use a smaller pressure range because of the finite signal-to-noise ratio (SNR) at very low and very high pressures. The surface of the membrane is observed by an imaging interferometer using continuous light, see Ref. 23. The observed interference pattern represents the surface profile of the sample as exemplified in Fig. 1(c). In principle, a high amplitude gives a high SNR. However, when the oscillation amplitude exceeds a few percent of the light wavelength, the contrast of the interference pattern is reduced. For an amplitude of about 20% of the

light wavelength, the contrast vanishes completely, as visible in two areas in Fig. 1(c). Below this threshold, the interference fringes can be used to quantitatively measure the vibrational amplitude. For measuring resonance curves, it is therefore necessary to adjust the amplitude of the excitation when varying the frequency to keep the amplitude in a suitable measurement range. Fig. 1(d) shows a measurement example for the (2,2) eigenmode with a well-adjusted amplitude.

The oscillations excited by piezo ring are coupled into the silicon chip and lead to an oscillation of the mechanical support of the membrane that itself excites the membrane to oscillate. An example of such a measurement for a membrane with a lateral size of roughly $400 \times 400 \mu\text{m}^2$ and a thickness of 400 nm is shown in Fig. 2(a). The different curves correspond to resonance curves measured at different pressures corresponding to the same color code as in Fig. 3 that we will discuss below. The frequency range is adapted to the width of the resonance curve. We observe a pronounced decrease of the resonance width when lowering the pressure, indicating that at high pressure the oscillations are damped by viscous friction with the air environment. Panel (a) shows that for low pressure the amplitude $|A|$ features a pronounced resonance around $f = 1.023$ MHz superimposed by small amplitude fluctuations throughout the whole frequency range. These background oscillations are attributed to the excitation system, while the resonance is identified as the (1,2) mode of the membrane. A zoom into the resonance is shown in the inset of panel (a). At higher pressure the background oscillations are of comparable size than the resonance itself, thereby hiding the shape of the resonance. In the following we describe how the contributions of membrane resonance and excitation system can be disentangled.

III. DATA ANALYSIS

A. Free-fitting model

We do not attempt to understand the mechanical details of the highly complex excitation system consisting of the piezo, the supporting metal block, the chip as well as the glue films in between. We will refer to it as the “excitation system” and to its resonance amplitude as $A_{\text{exc}}(\omega)$ in the following description. Its properties change from sample to sample, because of their dependence on the coupling strength of the sample to the excitation system. Instead we will present how they can be determined from the total response of the system. Three preconditions have to be fulfilled for the method to be applicable: (1) The amplitude of the excitation system shows a linear dependence on V_{AC} . This requirement is fulfilled for small and moderate V_{AC} . (2) Effects of the surrounding atmosphere on the excitation system are negligible. This assumption is justified because of its high mass and low surface area. (3) Feedback by the membrane motion on

the excitation system is negligible. This is fulfilled for a sufficiently large mass ratio between the excitation system and the membrane. In our case it amounts to five orders of magnitude.

As a consequence of linearity, the oscillation amplitude of the mechanical support of the membrane is a product of a function $A_{\text{exc}}(\omega)$ and V_{AC} . Since the excitation system resonance $A_{\text{exc}}(\omega)$ is assumed not to depend on properties of the atmosphere or of the membrane, mentioned as precondition (2) and (3), it is a pure function of ω .

If the amplitudes are sufficiently small, the membrane can be modeled as a linear oscillator. Therefore the total absolute amplitude $|A|$ of the membrane oscillation is a product of the resonance $A_{\text{memb}}(\omega)$ of an isolated membrane and the oscillation amplitude of the excitation system

$$|A| = A_{\text{memb}}(\omega) \cdot A_{\text{exc}}(\omega) \cdot V_{\text{AC}}. \quad (1)$$

In Eq. (1), only $|A|$ and V_{AC} are known from the experiment. For A_{memb} the well known resonance curve of a damped driven harmonic oscillator is assumed

$$A_{\text{memb}} = \frac{S}{\sqrt{(\omega^2 - \omega_0^2)^2 + 4\beta^2\omega^2}}, \quad (2)$$

with an eigenfrequency ω_0 , a damping constant β and a proportionality factor S measuring the coupling strength between the membrane oscillation and the excitation oscillation provided by the piezo ring. In the following, we present a way to separate the membrane resonance A_{memb} from the excitation system resonance A_{exc} and to obtain the parameters ω_0 , β and S .

The amplitude $|A|$ is measured as a function of ω for N different pressures p_i of the surrounding atmosphere, and $|A|_i$ is the corresponding amplitude. The parameters ω_{0i} , β_i and S_i in Eq. (2) for A_{memb} as well as the excitation voltage $V_{\text{AC}i}$ are also allowed to be pressure dependent. If all the parameters are given, $A_{\text{exc}}(\omega)$ can be calculated:

$$\begin{aligned} A_{\text{exc}}(\omega, \{\omega_{0i}\}, \{\beta_i\}, \{S_i\}) \\ = \sum_{i=1}^N W_i(\omega, \{\omega_{0i}\}, \{\beta_i\}, \{S_i\}) \\ \cdot \frac{|A|_i(\omega)}{A_{\text{memb}}(\omega, \omega_{0i}, \beta_i, S_i) V_{\text{AC}i}}. \end{aligned} \quad (3)$$

According to Eq. (1) the fraction on the bottom right is equal to $A_{\text{exc}}(\omega)$ for each addend. Therefore the weighted average using a weight function with $\sum_i W_i \equiv 1$ is also equal to $A_{\text{exc}}(\omega)$. The choice of W_i is arbitrary. We use

$$\begin{aligned} W_i(\omega, \{\omega_{0i}\}, \{\beta_i\}, \{S_i\}) &= \frac{w_i(\omega, \omega_{0i}, \beta_i, S_i)}{\sum_j w_j(\omega, \omega_{0j}, \beta_j, S_j)} \\ w_i(\omega, \omega_{0i}, \beta_i, S_i) &= \frac{A_{\text{memb}}(\omega, \omega_{0i}, \beta_i, S_i)}{\max_{\omega'} [A_{\text{memb}}(\omega', \omega_{0i}, \beta_i, S_i)]} \end{aligned}$$

with $\max_{\omega} [A_{\text{memb}}]$ denoting the maximum of the membrane resonance curve. This choice of the weight function

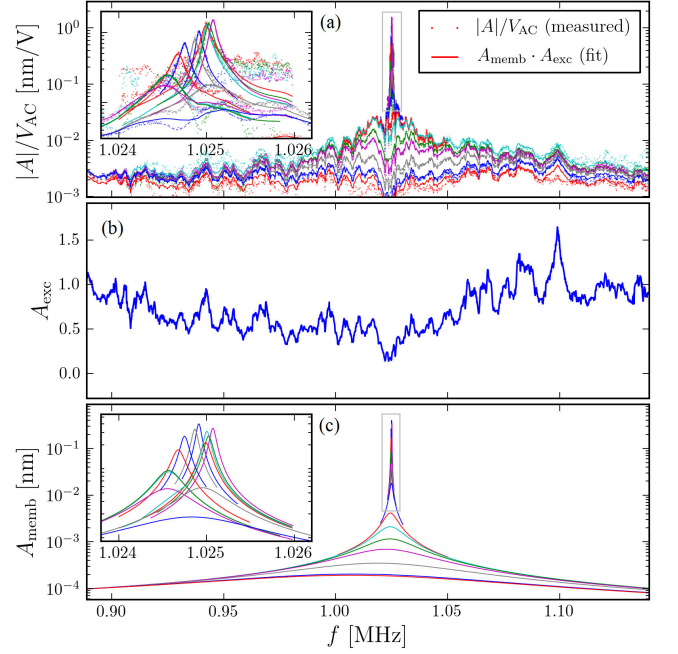


FIG. 2: (a) Measured resonance curves (i.e., oscillation amplitudes normalized by the excitation voltage as a function of frequency of a Si_3N_4 membrane (400 nm thick and lateral size of $416 \times 398 \mu\text{m}^2$)) are shown as dots. Each curve corresponds to a different atmospheric pressure in a range of almost 5 orders of magnitude from 1.6×10^{-2} mbar for the highest to 992 mbar for the lowest curve. For a quantitative scale of pressures see Fig. 3 where the same color code is used. The solid lines are results of a fit of $|A|_j(\omega)$ which is defined in the supporting information. The curves are shown for a selection of pressures to enhance clarity. (b) Amplitude of the excitation system A_{exc} defined in the supporting information. The product $A_{\text{memb}} \cdot A_{\text{exc}}$ (solid lines in (a)) is used to fit the experimental data. (c) Membrane resonance amplitudes A_{memb} . The inset shows a magnified view of the low pressure peaks located inside the light gray rectangle in the main panel.

is advantageous, because data points with high amplitude and therefore higher signal-to-noise ratio are given a higher weight. In Fig. 2 the factors of Eq. (1) deduced by this analysis are plotted as a function of the excitation frequency. The dimensionless response of the excitation system, A_{exc} , shown in panel (b) fluctuates around an average of 0.55, but has no pronounced feature in the relevant frequency range. Panel (c) displays the corrected response of the membrane A_{memb} , where now the resonance is clearly discernable also for high pressures.

In Eq. (1) A_{memb} and A_{exc} depend on the parameters $\{\omega_{0i}\}$, $\{\beta_i\}$ and $\{S_i\}$. Therefore it can be used to find

the best fit values for $\{\omega_{0i}\}$, $\{\beta_i\}$ and $\{S_i\}$:

$$\forall j: |A|_j(\omega) = A_{\text{memb}}(\omega, \omega_{0j}, \beta_j, S_j) \cdot A_{\text{exc},0}(\omega, \{\omega_{0i}\}, \{\beta_i\}, \{S_i\}) \cdot V_{\text{AC}} \quad (4)$$

$$\text{with } A_{\text{exc},0}(\omega, \dots) = \frac{A_{\text{exc}}(\omega, \dots)}{\langle A_{\text{exc}}(\omega', \dots) \rangle_{\omega'}}$$

where $A_{\text{exc},0}$ is A_{exc} normalized by its respective, pressure dependent frequency average. If $(\{\omega_{0i}\}, \{\beta_i\}, \{S_i\})$ is a solution, without normalization, using A_{exc} instead of $A_{\text{exc},0}$ in Eq. (4), $(\{\omega_{0i}\}, \{\beta_i\}, \{cS_i\})$ with an arbitrary constant $c \neq 0$ will also be a solution, since A_{memb} in Eq. (2) is proportional to c and A_{exc} in Eq. (3) is proportional to $1/c$. This ambiguity is avoided by the normalization of A_{exc} to $A_{\text{exc},0}$.

A least-square optimization algorithm is used to compute an approximate solution for $\{\omega_{0i}\}$, $\{\beta_i\}$ and $\{S_i\}$. The number of free parameters is $3N$, but can be reduced by forcing additional constraints on the so far independent parameters, as we will demonstrate in later discussion.

A graph of the best fit parameters for a fit with $3N$ free parameters as a function of pressure is shown as colored dots in Fig. 3. Instead of the damping parameter β the equivalent but more accessible quality factor $Q = \omega_0/\beta$ is shown in the upper panel. The Q factor increases by almost 4 orders of magnitude when lowering the pressure from atmospheric pressure to 50 mbar. At very low pressure ($p < 0.05$ mbar) the Q factor saturates, indicating that the remaining damping is given by intrinsic properties of the sample. In the second panel, the resonance frequency of the corresponding undamped oscillator $f_0 = \omega_0/2\pi$ is shown. f_0 is almost independent of pressure up to values of $p \simeq 30$ mbar. For higher pressure it decreases, indicating that the strong damping limit is approached. Since the parameters S_i strongly depend on the normalization of $A_{\text{exc},0}$ of each membrane resonance curve, and $A_{\text{exc},0}$ a group of N curves denotes which a matrix, we show instead in panel (c) of Fig. 3 the more descriptive effective excitation amplitude of the membrane frame $A_{\text{exc,eff}}$, which is defined as follows: Comparing Eq. (1) and (2) to the well known formulas of the driven damped harmonic oscillator, we conclude that the amplitude of the excitation system is $S_i A_{\text{exc}}(\omega) V_{\text{AC}}/\omega_0^2$. The effective amplitude is defined as the excitation system amplitude averaged using A_{memb} as a weight function

$$A_{\text{exc,eff},i} = \frac{\int d\omega [A_{\text{memb}}(\omega, \dots) \cdot \frac{S_i A_{\text{exc}}(\omega) V_{\text{AC}}}{\omega_0^2}]}{\int d\omega A_{\text{memb}}(\omega, \dots)} \quad (5)$$

The $A_{\text{exc,eff}}$ of the excitation system has a similar pressure dependence as V_{AC} , as anticipated. V_{AC} , shown in Fig. 3(d) was varied roughly linearly with pressure to keep the absolute amplitude within a similar range. The effective amplitude factors $S_{i,\text{eff}}$ in panel (e) are defined as:

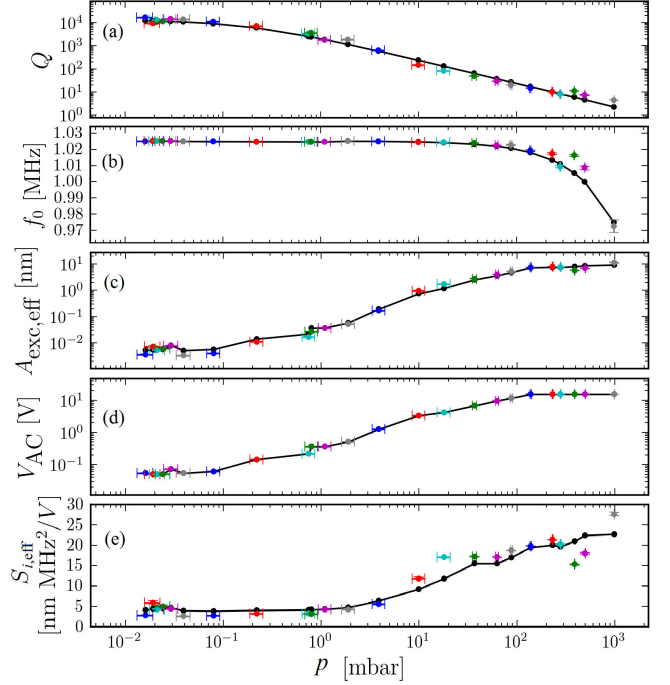


FIG. 3: Visualization the fit parameters as a function of the pressure of the surrounding atmosphere. The colored dots show the results of a fit with $3N$ free parameters. The color of the dots is the same as that of the corresponding curves in Fig. 2. The black dots and lines correspond to a fit with additional constraints, see text. The horizontal error bars are determined from the experimental values of the pressure sensors and the vertical error bars correspond to the Full Width at Half Maximum (FWHM) of the resonance curves. The quality factor Q is plotted in panel (a), the eigenfrequency of the corresponding undamped oscillator $f_0 = \omega_0/2\pi$ in panel (b), $A_{\text{exc,eff}}$ in panel (c), and the excitation voltage V_{AC} in panel (d). The proportionality factors $S_{i,\text{eff}}$ corresponding to the coupling strength between the excitation oscillation and the membrane oscillation are plotted in panel (e).

$$S_{i,\text{eff}} = \frac{A_{\text{exc,eff},i}}{V_{\text{AC}}} \cdot \omega_0^2 \quad (6)$$

This first analysis shows that for a given pressure the resonance curves can successfully be decomposed into the contribution of the excitation system and the system itself, justifying the assumptions made at the beginning. However, this free fitting with $3N$ parameters does not reveal the reasons for the pressure dependence of Q and f_0 . To do so, several additional constraints that relate the fitting parameters deduced for the individual pressure values can be applied.

B. Fitting with constraints

Imposing constraints reduces the number of independent fitting parameters. In the free-fitting model with $3N$ free parameters, S_i , f_0 , and β are all individual parameters for each pressure value. To demonstrate the impact of the constraints, we use the following three, physically motivated constraints: 1) If the coupling between the excitation system and the membrane was independent of pressure, S should be single-valued throughout the whole excitation range. We set here the slightly relaxed constraint of one S_1 per excitation voltage decade. In the given example this constraint reduces the number of independent fitting parameters from $3N = 72$ (for 24 pressure values measured) to $2N + 4$, since V_{AC} is varied over four orders of magnitude. 2) Above a certain pressure threshold (1.5 mbar in the present case) we assume a linear decrease of f_0 , reducing the number of independent parameters by the number of measurement points above the pressure threshold, plus 1 to describe the linear decrease. In the present case to $2N - 2 = 46$, since 7 data points are above the threshold. 3) Finally, the third constraint is that β is a linear function of the pressure, corresponding to viscous friction, resulting in a final number of $N = 24$ independent fitting parameters.

As presented in Fig. 3, the black dots and lines represent the fitting results when using all three additional constraints. We obtain a general good agreement between the fitting results of the free and the constrained model, except for the undamped eigenfrequency f_0 in the high pressure range $50 < p < 500$ mbar, where the freely fitted results are systematically higher than the constrained ones. In this pressure range the amplitude of the membrane oscillation is relatively small compared to A_{exc} , increasing the uncertainty with which f_0 can be determined. Still, the error bar is smaller than the deviation, meaning that at least one of the three constraints is not well justified. We argue that constraint 2), (the linear decrease of f_0) might be oversimplified. Nevertheless, the trends are well-reproduced by the constrained fitting, supporting the assumption that the membrane behaves as an harmonic oscillator.

In the model with additional constraints, different combinations of constraints and therefore different numbers of independent fitting parameters and different fitting results are possible. Of course, other constraints can also be chosen to test the applicability of other models and the physical relations between the parameters. Once a function of a specific physical model such as defects, crystallization and temperature dependent stress of the membrane has been established, it can be utilized as a constraint. The validity of such a constraint can be verified by comparing the accuracy of the fitting results between the maximum number of free parameters and the constrained model. When constraints describe the physical system inaccurately, the fitting results will deviate systematically from the free-fitting model.

IV. RESULTS AND DISCUSSION

A. VICL test results: quality factor and eigenfrequencies

We now apply this method to the ground mode and an excited mode of a 478 nm thick Si_3N_4 membrane with a lateral size of $298 \times 296 \mu\text{m}^2$.

Figure 4 shows the results for the ground mode (labeled the (1,1) mode, because it has one maximum in x and one in y direction) of a membrane. In Fig. 4(a) and (c), each curve represents a specific pressure: a lower pressure gives rise to a sharper peak with a higher amplitude. We also observe a slight shift of the resonance to higher frequencies with decreasing pressure in the low-pressure range, in contrast to the behavior of a damped harmonic oscillator. At very low pressure even non-monotonic behavior of the resonance frequency on the pressure may occur. We will comment on these two effects in the following description. The frequency dependence of the amplitude of the excitation system A_{exc} is presented in panel (b) of Fig. 4. The fit results of the Q factor in Fig. 4(d) increase with decreasing pressure as expected, if the damping is dominated by the air environment. At low pressure, the Q factor saturates, indicating that the intrinsic damping of the membrane starts to dominate. From the extrapolation to low pressure the intrinsic Q factor and the eigenfrequency of the ground mode (1,1) are estimated as $Q = 2 \times 10^4$ and $f_0 = 0.447$ MHz, respectively. By comparing with the theoretical eigenfrequencies expression: $f_{m,n} \simeq \sqrt{\sigma(m^2 + n^2)/(4\rho L^2)}$, where σ , ρ , L and (m, n) correspond to the tensile stress, mass density, lateral size of the membrane and the integer mode indices representing the number of antinodes, respectively [19, 20], with the values $\sigma = 1.099 \times 10^{-1}$ GPa (measured by our phase shifting and surface amplitude method [6]), $\rho = 3180$ kg/cm³, and $L \simeq 3.0 \times 10^{-4}$ m, for the (1,1) mode, we obtain $f_{1,1} \simeq 0.438$ MHz, which is 2.0% lower than our fitting results.

Now we discuss the excited (2,2) mode which has resonance frequencies around 1 MHz. Curves measured in a pressure range from 120 mbar to 0.091 mbar are plotted in Fig. 5(a). Due to the relatively small amplitude of this mode, the limited SNR, and the very large width of the resonance curves, measurements at higher pressures are not possible. Similarly, at low pressure very small excitation amplitudes have to be used to stay in the linear oscillator regime. When increasing the excitation, the shape of the resonance curves starts to deviate from the Lorentz curve shape. As a result the accessible frequency range is limited. As before, the contributions of the membrane and the excitation system are separated by the VICL analysis. The eigenfrequency of the (2,2) mode is estimated as $f_0 = 0.909$ MHz. For the (2,2) mode, $f_{2,2} \simeq 0.876$ MHz can be determined by the theoretical eigenfrequency equation with a discrepancy of 3.72% compared with the fitting results.

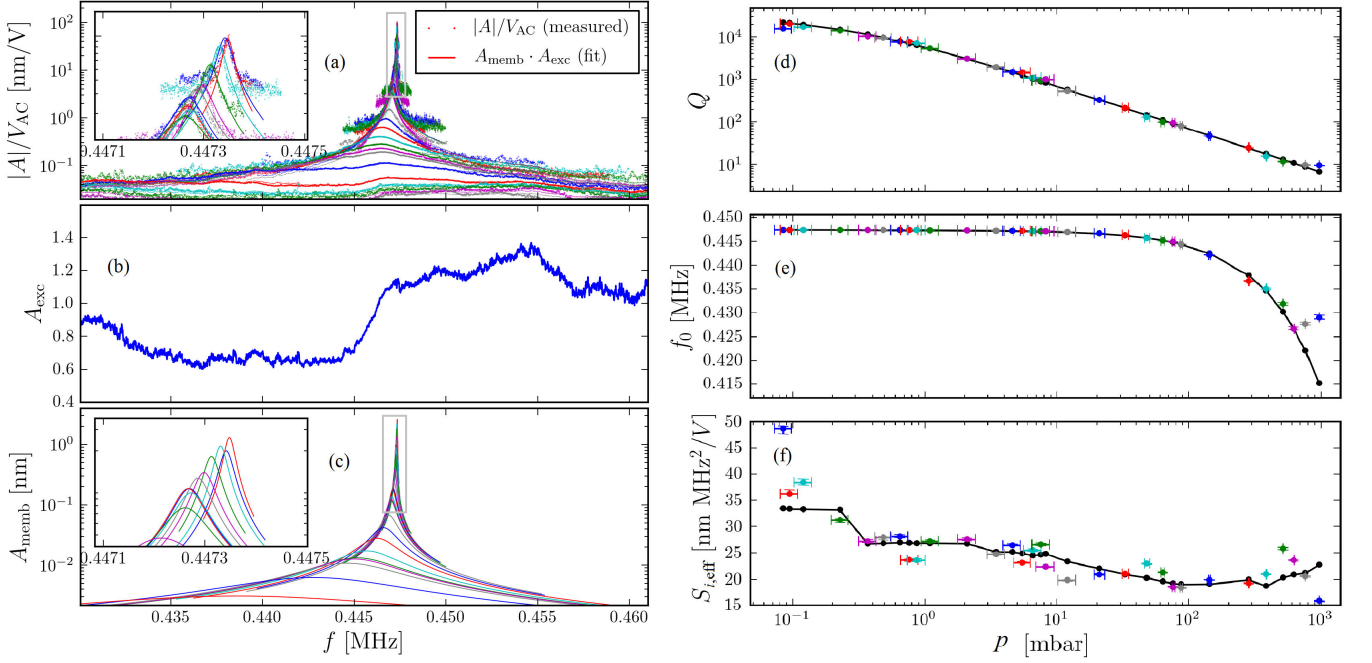


FIG. 4: Fitted VICL result of the ground mode (1,1) vibration of the Si_3N_4 membrane at 0.447 MHz. The measured resonance curves under different pressures with their individual fitting are plotted in (a). The separated A_{exc} and A_{memb} are plotted in (b) and (c), respectively. (d) Fitted curve of Q factor of the ground mode (1,1) vibration of the Si_3N_4 membrane at 0.447 MHz. (e) Eigenfrequency of the corresponding undamped oscillator f_0 . (f) Proportionality factors $S_{i,\text{eff}}$ corresponding to the coupling strength between the excitation oscillation and the membrane oscillation. Black dots and lines plotted in subfigure (d - f) represent the corresponding constraint fitting results.

Figure 5(e) shows a significant shift of f_0 of the (2,2) mode in higher frequencies when the pressure is lowered. This blue shift amounts to roughly 0.5 kHz below $p = 3$ mbar and is much more pronounced than for the (1,1) mode that increases by roughly 0.1 kHz in the same frequency range. In Fig. 5(d), the low-pressure limit of the Q factor of the membrane is estimated to be $Q = 2 \times 10^4$, in agreement with the results for the (1,1) mode and other modes for the same membrane (not shown). It also fits well with the observed scaling with $(L/h)^2$ reported in Ref. 19, from where we extrapolate our membrane to have a Q factor around 1.5×10^4 . This agreement indicates that the leveling off of Q at low pressure signals indeed the onset of intrinsic damping. The decrease of Q with increasing pressure for the (2,2) mode is weaker than for the (1,1) mode, such that in general the (2,2) mode has a higher Q factor than the (1,1) mode, indicating that the viscous damping of the environment is more effective for the ground mode. This behaviour can be understood since the integral displacement in the ground mode is much bigger than in the excited (2,2) mode.

We now turn to the constrained fitting. The fitting results of the constrained model (black dots and lines in the right panels of Fig. 4 and 5) approximately follow those of the free fitting model. However, the fitting results for the eigenfrequency of the (2,2) mode in the higher pressure range, as shown in Fig. 5(e), deviate systematically from the free-fitting results, indicating that constraint

2) does not accurately describe the experiment in that range, probably due to the mechanism described above. Another contributing possibility would be an enhancement of the effective mass of the membrane due to the inertia of the surrounding atmosphere, as observed earlier for Si membranes [6]. The $S_{i,\text{eff}}$ presented in panel (f) of Fig. 4 and 5 show a relatively weak dependence on pressure, supporting the harmonic oscillator model, in which a constant S is expected. For the (1,1) mode the constrained fit results agree well with the free-fitting results, except for the two data points at the extremes of the pressure range. For the (2,2) mode the $S_{i,\text{eff}}$ values of the free and the constraint model both scatter around a constant value, and the deviation between freely-fitted results and constrained results is smaller than the scatter. We attribute the scatter to the small overall amplitude which is a factor of 25 smaller than for the (1,1) mode.

B. Temperature dependent resonance frequencies

We now turn to a possible explanation of the frequency shifts and increased scattering, especially in the lower pressure range, which are directly presented in Fig. 5(c) and 5(e). The f_0 in the weak damping regime at low pressure should be approximately constant according to the expression of the damped driven harmonic oscillator in Eq. (2). Possible reasons for the frequency shift in-

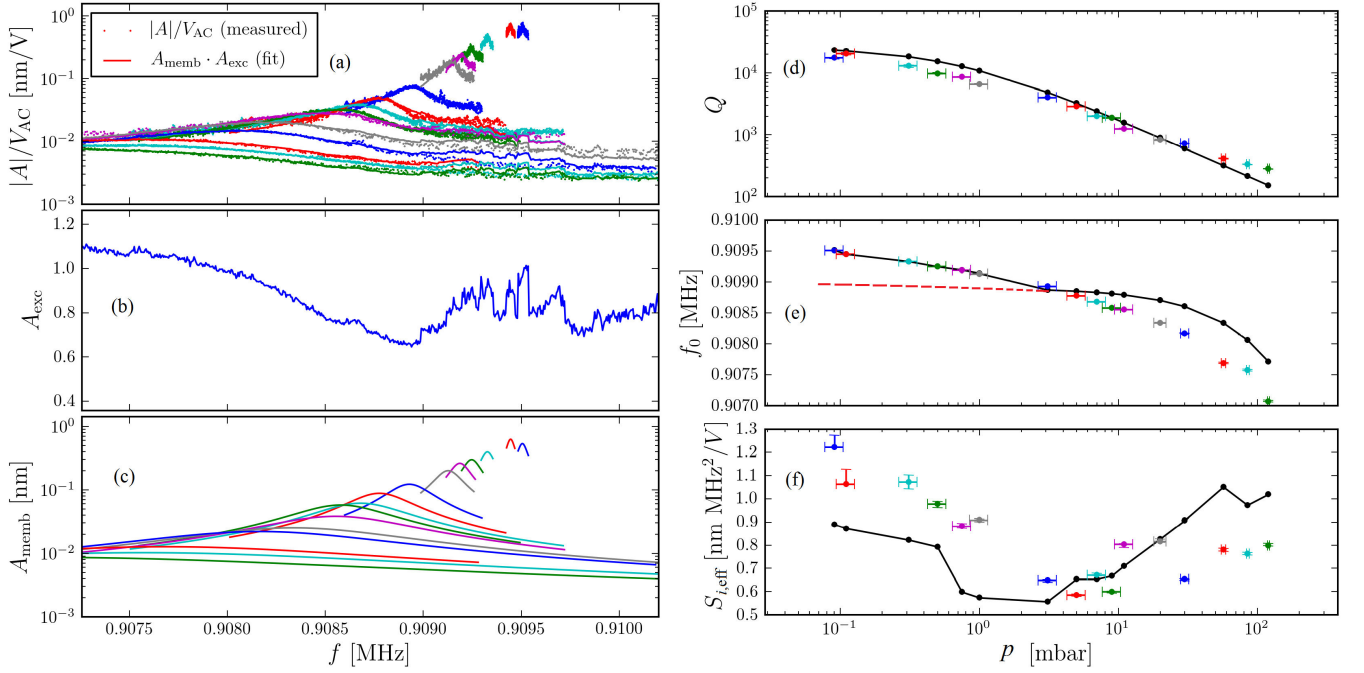


FIG. 5: VICL results: fitted of the (2,2) mode vibration of the Si_3N_4 membrane at 0.909 MHz. The measured resonance curves under different pressures with their individual fitting are plotted in (a). The separated A_{exc} and A_{memb} are plotted in (b) and (c), respectively. (d) Fitted curve of Q factor of the (2,2) mode vibration of the Si_3N_4 membrane at 0.909 MHz. (e) Eigenfrequency of the corresponding undamped oscillator f_0 . (f) Proportionality factors $S_{i,\text{eff}}$ corresponding to the coupling strength between excitation oscillation and membrane oscillation. Black dots and lines plotted in subfigure (d - f) represent the corresponding constraint fitting results.

clude the following: When running a complete VICL test at room temperature which takes about 3 hours under continuous heat input, at low pressure the temperature might not be constant. Further potential error sources are the finite precision of the pressure measurement and the stability of the electro-mechanical performance of the piezo ring. However, the pressure sensors are well calibrated and the contribution of the excitation system including the piezo ring is separated and extracted by our analysis. Thus we argue that the temperature variation might cause a slight shift of the eigenfrequency. To quantify this effect we study the sensitivity of the response curves of the ground mode of a Si_3N_4 membrane to temperature changes, as shown in Fig. 6. We placed the sample holder on an auto-controlled heating stage to adjust the temperature of the sample. The resolution of the temperature control stage is 1°C . The heating stage is placed under the vacuum chamber and heats the whole vacuum stage to the set temperature. Temperatures are directly measured by the sensor which is fixed in the copper stage and next to the sample. Since the interference pattern is highly sensitive to any changes of the geometry caused by thermal nonequilibrium (thermal expansion, temperature gradients, etc.), we use the camera of the interferometer to monitor the equilibration process, which may take up to 2 hours. When the interference pattern is stable in time we start the VICL measurements.

The curves have been measured for ascending temperatures in a moderate vacuum range of 3-4 mbar where the SNR is highest. The minimum setting temperature of the heating stage is 38.0°C . The resonance frequency shift between the lowest and the highest temperature is about 3.5 kHz with an approximately linear increasing relation between the temperature and the resonance frequency, presented in the inserted image of Fig. 6. Thus the resonance frequency shift can be averaged as $550 \text{ Hz}/^\circ\text{C}$. This increase may arise from the different thermal expansion coefficient of the silicon chip and the Si_3N_4 membrane [24] and will be studied in more detail in a forthcoming publication.

In Fig. 5(a) and 5(c), the frequency shift can be directly observed. The curves have been recorded for decreasing temperature. From 2 mbar down to 0.01 mbar f_0 increases by roughly 500 Hz. The temperature sensitivity indicated above was determined for the (1,1) mode. When assuming that the temperature change of f_0 scales with f_0 , we imply the temperature dependent resonance frequency measurement on (2,2) mode and we find the temperature sensitivity of the (2,2) mode of approximately $113 \text{ Hz}/^\circ\text{C}$, corresponding to a temperature increase of 4.4°C . Such a temperature increasing magnitude can well be caused by the heat dissipation of running equipments of the VICL test. We therefore attribute the deviations of these low-pressure data points to slight in-

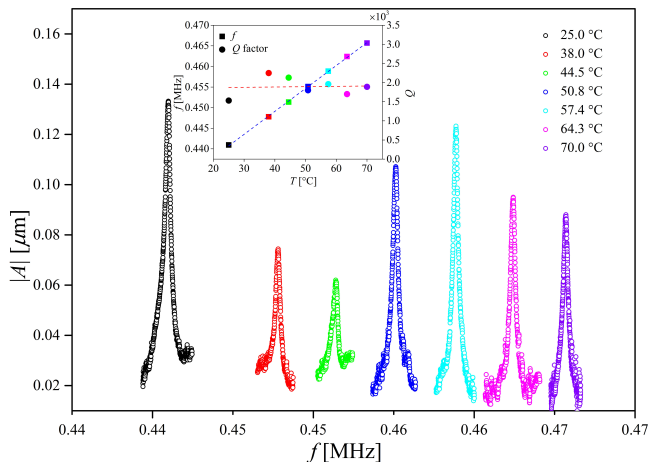


FIG. 6: Resonance curves of the ground mode vibration at different temperatures of the Si_3N_4 membrane.

Curves are measured in a close pressure range of 3-4 mbar in order to eliminate the frequency shift caused by different air damping. Temperatures are directly measured by the sensor which is fixed in the copper stage and next to the sample. Curves are measured at 25.0 °C, 38.0 °C, 44.5 °C, 50.8 °C, 57.4 °C, 64.3 °C and 70.0 °C. The values of the resonance frequencies fitted from the resonance curves measured at different temperatures are plotted in the inserted image. The colors of the dots correspond to those of the resonance curves. The values of the resonance frequencies follow a linear tendency illustrated by the linear fitting result (blue dashed line). The approximative values of Q factors estimated from the resonance curves at different temperatures with their linear fitting (red dashed line) are also plotted in the inset image. The error bars are smaller than the symbol size.

creases of the temperature. A constant temperature of the sample would result in the red dashed line in Fig. 5(e).

Figure 6 also shows that the Q factor is almost independent of temperature under these conditions. We deduce an average value of $1.9 \pm 0.4 \times 10^3$ agreeing well with the value observed at room temperature, as shown in Fig. 4(d). We conclude that in this temperature range the viscosity of the air and its resulting damping are constant. When operating the membrane resonator under these conditions, the FWHM of the ground mode amounts to approximately 200 Hz, meaning that temperature changes of 0.4 K are detectable. This high temperature sensitivity makes Si_3N_4 membrane resonators suitable as temperature sensors. For lower pressures and even higher temperature resolution is possible because of the higher Q -factor. For example, in Fig. 5(c), the resonance frequencies of the lowest two pairs of pressure values are shifted by 50 Hz and 130 Hz,

respectively, corresponding to a temperature variation of 0.44 °C and 1.15 °C, respectively.

V. CONCLUSION AND SUMMARY

In summary, we present a method to determine the eigenfrequencies and the Q factors of freestanding Si_3N_4 membranes at varying pressure by optical profilometry. This Vibrometry In Continuous Light (VICL) method uses the resonance curve of a damped driven harmonic oscillator to decompose the response of the membrane coupled to the excitation system into contributions of the membrane and of the excitation system alone. With the VICL method we determine the Q factors and the eigenfrequencies of individual vibration modes of a Si_3N_4 membrane. We compare the best-fit results obtained when fitting all individual resonance curves independently, with a constrained fitting imposing correlations between the fit results according to a damped linear oscillator with viscous friction. The eigenfrequencies of the (1,1) and (2,2) mode correspond well to the expected values for a bending plate. The low-pressure limits of the Q factors of these two modes are estimated to be 2×10^4 as expected for membranes with the given ratio of lateral size and thickness. Further investigations are necessary to reveal the nature of the intrinsic damping. We find that the (1,1) mode is well described by the harmonic oscillator model, while the (2,2) mode reveals deviations that we attribute to the finite accessible pressure and the frequency range due to the onset of nonlinear components for slightly higher excitation amplitudes. Small variations of the resonance frequency can be attributed to a slight temperature variation. In the intermediate pressure range, when air damping is dominant, but the SNR is high, the Q factor is independent of the temperature around room temperature. These two properties, the high sensitivity of the resonance frequency to the test environment temperature and the robustness of the Q factors open up the possibility to use the system as a highly sensitive temperature sensor.

ACKNOWLEDGMENTS

The authors thank Stephan Nößner and Michael Hertkorn for their contribution in the early phase of this project. We are indebted to Mike Hettich and the SFB767 Nanomechanics Discussion Group for fruitful discussion and comments about the manuscript. The authors thank the Deutsche Forschungsgemeinschaft for financial support through SFB767. This work was also supported by the China Scholarship Council.

-
- [1] J. Yang, X. Jiao, R. Zhang, H. Zhong, and Y. Shi, Acoustic Waves and Device Applications (SPAWDA), IEEE pp. 191–194 (2012).
 - [2] J. Lee, S. Kim, J. Lee, D. Yang, B. Park, S. Ryu, and I. Park, *Nanoscale* **6**, 11932 (1992).
 - [3] G. Sberveglieri, W. Hellmich, and G. Mueller, *Microsyst. Technol.* **3**, 183 (1997).
 - [4] M. G. Lagally, *MRS Bull.* **32**, 57 (2007).
 - [5] M. M. Roberts, L. J. Klein, D. E. Savage, K. A. Slinker, M. Friesen, G. Celler, M. A. Eriksson, and M. G. Lagally, *Nat. Mater.* **5**, 388 (2006).
 - [6] R. Waitz, S. Nöbner, M. Hertkorn, O. Schecker, and E. Scheer, *Phy. Rev. B* **85**, 035324 (2012).
 - [7] X. Zhang, R. Waitz, F. Yang, C. Lutz, P. Angelova, A. Götzhäuser, and E. Scheer, *Appl. Phys. Lett.* **106**, 063107 (2015).
 - [8] M. Tomi, A. Isacson, M. Oksanen, D. Lyashenko, J.-P. Kaikkonen, S. Tervakangas, J. Kolehmainen, and P. J. Hakonen, *Nanoscale* **7**, 14747 (2015).
 - [9] C.-H. Liu, I. S. Kim, and L. J. Lauhon, *Nano lett.* **15**, 6727 (2015).
 - [10] A. Castellanos-Gomez, R. van Leeuwen, M. Buscema, H. S. van der Zant, G. A. Steele, and W. J. Venstra, *Adv. Mater.* **25**, 6719 (2013).
 - [11] E. Kramer, J. van Dorp, R. van Leeuwen, and W. Venstra, *Appl. Phys. Lett.* **107**, 091903 (2015).
 - [12] J. Thompson, B. Zwickl, A. Jayich, F. Marquardt, S. Girvin, and J. Harris, *Nature* **452**, 72 (2008).
 - [13] D. Wilson, C. Regal, S. Papp, and H. Kimble, *Phys. Rev. Lett* **103**, 207204 (2009).
 - [14] K. Usami, A. Naesby, T. Bagci, B. M. Nielsen, J. Liu, S. Stobbe, P. Lodahl, and E. S. Polzik, *Nat. Phys.* **8**, 168 (2012).
 - [15] J. Park, H. Qin, M. Scalf, R. T. Hilger, M. S. Westphall, L. M. Smith, and R. H. Blick, *Nano lett.* **11**, 3681 (2011).
 - [16] J. Park, H. Kim, and R. H. Blick, *Nanoscale* **4**, 2543 (2012).
 - [17] P. H. Otsuka, K. Nanri, O. Matsuda, M. Tomoda, D. Profunser, I. Veres, S. Danworaphong, A. Khelif, S. Benchabane, V. Laude, et al., *Sci. Rep.* **3**, 3351 (2013).
 - [18] B. Zwickl, W. Shanks, A. Jayich, C. Yang, A. Jayich, J. Thompson, and J. Harris, *Appl. Phys. Lett.* **92**, 103125 (2008).
 - [19] S. Chakram, Y. Patil, L. Chang, and M. Vengalattore, *Phys. Rev. Lett* **112**, 127201 (2014).
 - [20] P.-L. Yu, T. Purdy, and C. Regal, *Phys. Rev. Lett* **108**, 083603 (2009).
 - [21] M. Schubert, M. Grossmann, C. He, D. Brick, P. Scheel, O. Ristow, V. Gusev, and T. Dekorsy, *Ultrasonics* **56**, 109 (2015).
 - [22] R. Waitz, C. Lutz, S. Nöbner, M. Hertkorn, and E. Scheer, *Phys. Rev. Applied* **3**, 044002 (2015).
 - [23] S. Petitgrand, R. Yahiaoui, K. Danaie, A. Bosseboeuf, and J. P. Gilles, *Opt. Laser Eng.* **36**, 77 (2001).
 - [24] A. Sinha, H. Levinstein, and T. Smith, *J. Appl. Phys.* **49**, 2423 (1978).